2021 43rd Annual International Conference of the
IEEE Engineering in Medicine & Biology Society (EMBC)
Oct 31 - Nov 4, 2021. Virtual Conference

Computational Modeling of an Endovascular Peripheral Nerve Interface

JingYang Liu, David B. Grayden, *Senior Member, IEEE*, Janet R. Keast, Sam E. John, *Member, IEEE*

***Abstract*— Implantable neuromodulation devices that interface with the peripheral nervous system are a promising approach to restore functions lost to nerve damage. Existing nerve stimulation electrodes require direct contact with the target nerve and are associated with mechanical nerve damage and fibrous tissue encapsulation. Endovascularly delivered electrode arrays may provide a less invasive solution. Using a hybrid tissue conductor-neuron model and computational simulations, this study demonstrates the feasibility of delivering electrical stimulation of a peripheral nerve from a blood vessel in the vicinity of the target and predicts that the stimulation intensity required strongly depends on nerve-vessel distance and relative orientation, which are important factors to consider when screening candidate blood vessels for electrode implantation.**

I. Introduction

A significant amount of effort in recent years has been applied to the development of implantable peripheral nerve interfaces (PNIs). Interfacing with the peripheral nervous system provides an opportunity to restore motor, sensory, and autonomic functions that may be impaired due to disease or injury by stimulation of efferent and afferent fibers. Recent explorations of PNI clinical applications include control of neuroprosthetic limbs, rehabilitation, restoration of sensation, and modulation of autonomic functions [1].

Most existing peripheral nerve electrical stimulation devices use extra-neural electrodes that are positioned in direct contact with the target nerve, such as cuff electrodes [2], flat-interface electrodes [3], and book electrodes [4]. Such modalities have the advantage of localizing current spread and low electrode impedance, leading to high selectivity towards target nerve fascicles. However, damage to the nerve may be inflicted through constriction, traction, or relative motion of the electrodes [1]. Furthermore, foreign body reaction to chronically implanted electrodes leads to fibrotic encapsulation of the foreign material even when the electrodes are stimulated at safe levels [5]. The layer of fibrotic tissue adds a resistive barrier around the electrodes, shunting current and altering the distribution of the electric field, which consequently reduces stimulation efficiency and selectivity and the quality of recorded signals [5, 6].

Endovascular electrode placement has been explored for recording [7, 8] and stimulating [9] cortical neural activity as an alternative to surgically implanted intracranial electrodes. The implantation procedure is minimally invasive and the lack of direct nerve-electrode contact circumvents mechanical mismatch and relative motion between the implant and nerve tissue, thereby mitigating fibrotic encapsulation [11].

Recently, the application of endovascular neuromodulation has expanded to the peripheral nervous system. Endovascular PNIs have shown promising outcomes in a chronic clinical setting for central sleep apnea treatment [12] and in an acute pre-clinical setting for reducing ventricular rate to prevent arrhythmias during acute myocardial ischemia [13]. Despite its safety advantages, endovascular neuromodulation continues to be constrained by the availability of a suitable blood vessel near the target nerve and is limited by the course and distance of the vessel from the nerve. Teplitzky et al. [14] developed a computational model to investigate the feasibility of endovascular deep brain stimulation, but no study has focused on the feasibility of electrical stimulation of a peripheral nerve from an endovascular PNI.

In this study, we performed computational modeling to investigate the selection criteria of a suitable blood vessel for an endovascular PNI. The Stentrode™ (Synchron, Inc, USA) is a recently developed electrode array mounted on a self-expanding stent that can endovascularly record cortical signals [7, 8] and focally stimulate the cortex [9]. An idealized, three-dimensional model was constructed consisting of a peripheral nerve, a nearby vein and two endovascular disc electrodes modeled after the Stentrode design. The human pelvic splanchnic nerves (PSNs) were selected due to their potential as a stimulation target for graded bladder contraction control as well as the technical difficulties associated with cuff electrode placement [15]. Sim4Life provides direct coupling of electromagnetic field simulation with neuronal dynamics modeling. The effects of the location and relative orientation of the vessel were investigated by estimating the simulated stimulation intensity required to excite PSN motor axons by the endovascular electrodes.

II. Methods

A hybrid finite element method (FEM) conductor-neuron model was implemented using Sim4Life 6.0 (ZMT Zürich MedTech AG, Switzerland). The inhomogeneous conductor model consisted of neural tissue with simplified geometry, a nearby vein, endovascular disc electrodes, and a saline environment surrounding the key anatomical features, as shown in Fig. 1. Because histological sections showing the precise fascicular anatomy of human pelvic splanchnic nerve (PSN) arising from the S3 sacral roots are not available, an idealized model of the PSN was developed based on anatomical descriptions reported by past studies.

A cylindrical volume conductor centered at the mid-point between the nerve and vessel represented the saline

JingYang Liu is with The University of Melbourne, Victoria 3053, Australia. (email: jingyangl2@student.unimelb.edu.au)

David B. Grayden, Janet R. Keast and Sam E. John are with the University of Melbourne, Victoria 3053, Australia.

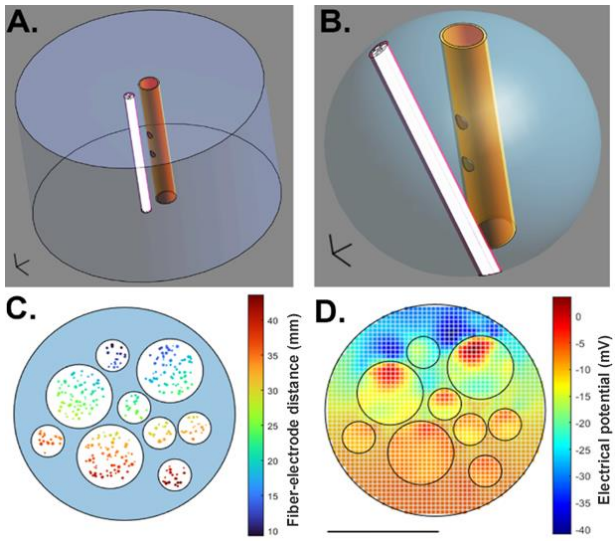

Fig. 1. FEM conductor-neuron hybrid model. A: The FEM model showing the target nerve (PSN, white) and nearby vein with two endovascular disc electrodes (orange), encased in a saline cylinder (blue). B: In a spherical saline boundary, the nerve can be rotated about the center of the saline volume in a plane parallel to the nearby vein. Scale: 1 mm. C: Cross-section at a nerve end showing a random arrangement of the fascicles and axons. Marker size corresponds to axon diameter; marker color corresponds to fiber-electrode distance. D: Electrical potential distribution within a nerve cross-section near the cathodic electrode. Color corresponds to local electrical potential.

intraoperative environment (Fig. 1A). A zero-flux Neumann boundary condition was set at the outermost surface of the saline volume. The error introduced by approximating an infinite tissue volume with a finite cylindrical structure was investigated using root mean square error (RMSE) [16]. A radius of 10 mm and a length of 15 mm were selected for the saline outer boundary; increasing each boundary dimension by 50% only changed the electrical potential distribution within the nerve by less than 1.5% and the axonal activation threshold by less than 4%. An unstructured mesh with tetrahedral elements was generated using the Sim4Life built-in multidomain mesh tool. Mesh element size was adjusted to be finer near the electrode and nerve anatomy, where the electrical potential gradient was high and coarser in the saline environment, resulting in a volumetric mesh of 7M elements.

To investigate the effects of relative rotation angle between the nerve and vessel, the cylindrical saline conductor layer was replaced by a spherical saline volume to allow nerve rotation (Fig. 1B). A similar sensitivity analysis was performed to determine the minimal sufficient saline boundary size. A saline layer radius of 12 mm was selected; increasing it by 50% changed the electrical potential distribution within the nerve by less than 2% and the axonal activation threshold by less than 5%. This boundary size led to a mesh of 2M elements.

A PSN third sacral root diameter of 1 mm was estimated from whole-mount staining images [17]. Here, the target PSN root was represented as a single nerve trunk containing multiple fascicles, interfascicular epineurium tissue, a perineurium tissue layer surrounding each fascicle, and anisotropic endoneurium tissue. Corresponding to observed composite nerve bundles [18], a total of nine round fascicles were modeled and randomly positioned in the nerve trunk, including three thick fascicles with diameter 300 µm and six intermediate fascicles with diameter 150 µm. There were 90 and 23 axon fibers randomly populated within each thick and intermediate fascicle, respectively (Fig. 1C). The fiber density was reduced by 50 times compared to histological observation to reduce computation load, but this did not affect the local electromagnetic field within each fascicle.

The perineurium was modeled as a highly resistive thin layer with a thickness of 3% of the fascicle diameter; thin nerve bundles less than 50 µm in diameter were excluded from this study due to their low resistance and, therefore, negligible influence on the activation of neighboring fascicles [19]. Since there is little data available on axon diameters of the human PSN, data measured from the anterior tibial nerve [20] and the sural nerve [21] were used to approximate a bimodal distribution ranging from 2 µm to 13 µm for the myelinated axons of the PSN, with a 40% incidence of large fibers (diameter > 6 µm) [17, 22]. As the goal of the present study was to investigate the activation of the efferent pathways of the PSNs via endovascular electrical stimulation, only myelinated axons were included in the model.

A nearby vein was constructed with a diameter of 2 mm, similar to that of the uterine vein [23] typically observed in the same pararectal space as the PSNs. A pair of compliant endovascular disc electrodes (750 µm diameter, 50 µm thickness, 2.5 mm apart) were modeled after the Stentrode design [7]. The struts of the stent were not included as they are not expected to contribute to the electrical stimulation.

Table 1 shows the conductivity values of different tissues in the model. For intraoperative activation of the bladder detrusor muscle, a pulse frequency lower than 35 Hz is often applied to human PSNs or pelvic nerves in animals [15, 24, 25]. As the electrodes and the target nerve are engulfed in body fluids that are good conductors, the ohmic current dominates the displacement current. Therefore, the electromagnetic low-frequency (EM LF) ohmic quasi-static solver was used to solve for the overall electromagnetic field within the target nerve (Fig. 1D). Neumann boundary conditions were assigned to the surfaces of the electrodes so that each electrode carried the same uniform current density distribution but the opposite polarity. In Sim4Life, the computed electromagnetic field is directly passed to the built-in NEURON solver (Yale University, CT, USA) and the neuronal activation is calculated using the local electrical potential gradient. The Sweeney

TABLE I.
CONDUCTIVITY VALUES OF MODELED TISSUES

Tissue	Conductivity (S/m)	Reference
Epineurium	8.3e-3	[27]
Perineurium	8.7e-4	[27]
Endoneurium (transverse)	8.8e-3	[28]
Endoneurium (longitudinal)	0.57	[28]
Blood	0.66	[29]
Vessel wall	0.38	
Saline	2.0	[29]

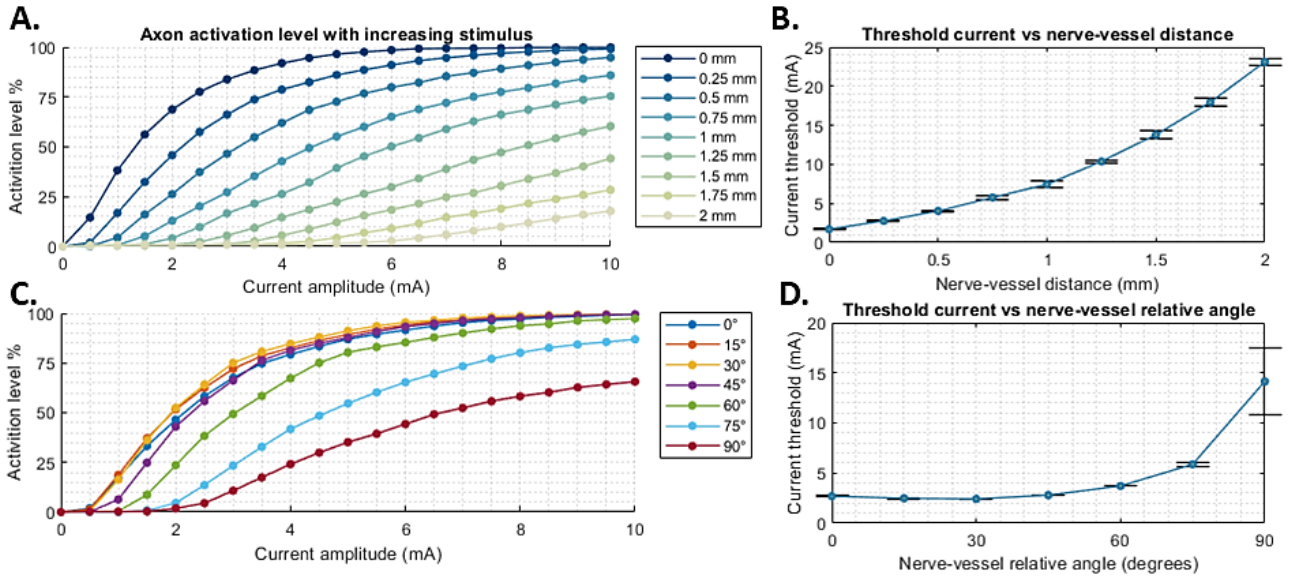

Fig. 2. Effects of nerve-vessel distance and relative orientation on axon activation shown as action profiles (A, C: mean of all fascicle arrangements tested) and population-average axonal activation threshold (B, D: mean ± standard deviation of all fascicle arrangements tested).

model of a myelinated mammalian peripheral nerve was used to describe the axonal dynamics. This model assumes that the internodal myelin is a perfect insulator, and the axon diameter at node and internodal length are linearly scaled to fiber diameter [26].

A biphasic, bipolar, cathodic-leading square current pulse with a phase width of 300 µs and no inter-phase delay was applied in the neuronal dynamics simulation to evoke action potentials. The titration function of Sim4Life was used to determine the axonal activation threshold current amplitude for each axon. Within the cylindrical saline boundary, the target nerve and vessel were held parallel to each other while the distance between them varied from 0 mm to 2 mm in increments of 0.25 mm. Within the spherical saline boundary, the nerve was rotated by up to 90 degrees relative to the mid-point between the endovascular electrode pair in a parallel plane at fixed nerve-vessel distance of 0.25 mm. The effects of the nerve-vessel distance and relative angle were investigated by assessing the axonal threshold stimulus current amplitude for each instance. To account for variability in neural anatomy, five different variations of fascicle positioning were tested for each instance, and differences among activation thresholds were tested with the Kruskal-Wallis test (alpha = 0.05).

III. Results

Axon activation profiles were generated for the entire axon population by calculating the percentage of axons activated at each stimulus current amplitude. Fig. 2A-B show the predicted activation profiles and axon population-average activation thresholds as the distances between the target nerve and vein vary from 0 mm to 2 mm, averaged from the results of five tested fascicle arrangements. For all tested fascicle arrangements, the stimulation intensity required to effectively recruit axons increased significantly with nerve-vessel distance. The simulated target nerve was easily activated by any non-zero stimulus amplitude when the electrode-bearing vessel was immediately adjacent at 0 mm, and a nearly 100% recruitment level was achieved with a current pulse amplitude of 6 mA. In contrast, at 2 mm distance, the target nerve model showed no activation until the stimulus amplitude reached 5.5 mA, and the overall axon activation level remained more than 80% lower at each stimulation intensity compared to the 0 mm distance. The activation threshold data did not follow a normal distribution, so a Kruskal-Wallis test was used to test the differences between results generated from different fascicle arrangements. The test result showed that fascicle arrangement did not significantly affect the activation threshold ($p = 0.9851$). The small standard deviations, ranging over 0.08-0.54 mA (Fig. 2B) also indicated that there was little variation in the axon activation thresholds with fascicle arrangement.

Fig. 2C-D show the predicted activation profile and average axonal activation threshold with relative nerve-vessel angle ranging from 0° to 90° with 0° representing parallel alignment of the nerve and vessel at 0.25 mm apart. Overall, the axonal activation threshold increased as the vessel approached an orthogonal orientation relative to the target nerve. When the relative angle was below 30°, this effect was

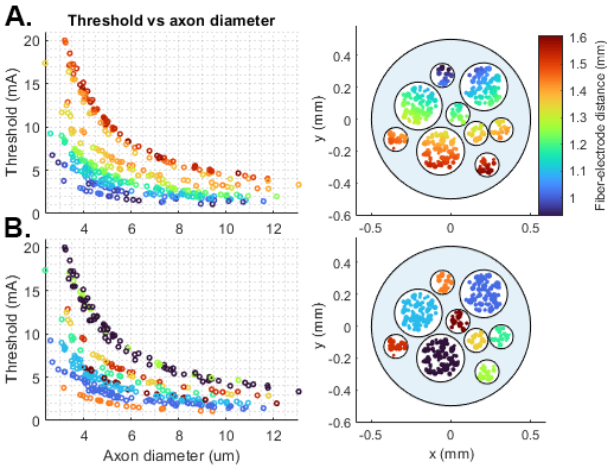

Fig. 3. Cross-sections of the modeled PSN and effect of axon-electrode distance (A) and fascicle thickness (B) on predicted activation threshold. Marker color corresponds to fiber-electrode distance in (A) and identifies axons in individual fascicles in (B).

not significant. The perpendicular orientation produced an average activation threshold more than 3.4 times greater than that of the parallel alignment in all tested fascicle arrangements. This reduction in stimulation efficacy was attributed to a combination of a slight increase in axon-electrode distance and a change in the fascicle orientation in relation to the electric field. The Kruskal-Wallis test did not show a significant difference between the five fascicle arrangements ($p = 0.9716$). The orthogonal orientation also introduced more variation in the activation profile. While the standard deviations between the activation profiles ranged over 0.03-0.19 mA with a nerve-vessel relative angle below 75°, the orthogonal orientation resulted in a standard deviation of 3.45 mA (Fig. 2D).

Fig. 3 shows the effect of absolute distance between the electrodes and each axon as well as fascicle size on axonal activation threshold. Since the axon fibers aligned perfectly parallel with the vessel and thus the line passing through the electrode centers, the activation threshold of each axon strongly and negatively correlated with its diameter (Fig. 3A), in accordance with commonly observed inverse recruitment observed in functional electrical stimulation devices. As shown in Fig. 3B, at similar distances, thicker fascicles required higher stimulation intensity as the resistive perineurium layer was thicker, which was in agreement with previous modeling studies [19].

IV. Conclusions

This modeling study demonstrates the feasibility of using an endovascular approach to electrically stimulate a peripheral nerve similar in size and composition to the human pelvic splanchnic nerve (PSN), with potential application in PSN stimulation for bladder control. The simulation results indicate that, when considering candidate blood vessels for electrode implantation, a closer distance to the target nerve as well as a smaller relative angle are preferred as these factors are predicted to increase the stimulation efficacy and significantly reduce the amplitude of stimulation required.

References

[1] Larson, C.E. & Meng, E., "A review for the peripheral nerve interface designer," Journal of Neuroscience Methods, vol. 15, p. 108523, 2020.

[2] Charkhkar, H., et al, "High-density peripheral nerve cuffs restore natural sensation to individuals with lower-limb amputations," Journal of Neural Engineering, vol. 15, p. aac964, 2018.

[3] Tyler, D.J. & Durand, D.M, "Functionally selective peripheral nerve stimulation with a flat interface nerve electrode," IEEE Transactions on Neural Systems and Rehabilitation Engineering, vol. 10, no. 4, pp. 294-303, 2002.

[4] Brindley, G.S., et al, "Sacral anterior root stimulators for bladder control in paraplegia," Spinal Cord, vol. 20, pp. 365-381, 1982.

[5] Grill, W.M. & Mortimer, J.T., "Electrical properties of implant encapsulation tissue," Annals of Biomedical Engineering, vol. 22, no. 1, pp. 23-33, 1994.

[6] Khurram, A., et al, "Chronic monitoring of lower urinary tract activity via a sacral dorsal root ganglia interface," Journal of Neural Engineering, vol. 14, p. aa6801, 2017.

[7] Oxley, T.J., et al, "Minimally invasive endovascular stent-electrode array for high-fidelity, chronic recordings of cortical neural activity," Nature Biotechnology, vol. 34, no. 3, pp. 320-30, 2016.

[8] John, S.E., et al, "Signal quality of simultaneously recorded endovascular, subdural and epidural signals are comparable," Nature Scientific Reports, vol. 8, p. 8427, 2018.

[9] Opie, N.L., et al, "Focal stimulation of the sheep motor cortex with a chronically implanted minimally invasive electrode array mounted on an endovascular stent," Nature Biomedical Engineering, vol. 2, pp. 907-14, 2018.

[10] Penn, R.D., et al, "Intravascular intracranial EEG recording," Journal of Neurosurgery, vol. 38, no. 2, p. 0239, 1973.

[11] Renz, A.F., et al, "A guide towards long-term functional electrodes interfacing neuronal tissue," Journal of Neural Engineering, vol. 15, p. aae0c2, 2018.

[12] Jagielski, D., et al, "Transvenous stimulation of the phrenic nerve for the treatment of central sleep apnoea: 12 months' experience with the remede System," European Journal of Heart Failure, vol. 18, pp. 1386-93, 2016.

[13] Inagaki, M., et al, "Intravascular parasympathetic cardiac nerve stimulation prevents ventricular arrhythmias during acute myocardial ischemia," in Engineering in Medicine and Biology 27th Annual Conference, Shanghai, China, 2005.

[14] Teplitzky, B.A., et al, "Computational modeling of an endovascular approach to deep brain stimulation," Journal of Neural Engineering, vol. 11, p. 026011, 2014.

[15] Peh, W.Y.X., et al, "Novel neurostimulation of autonomic pelvic nerves overcomes bladder-sphincter dyssynergia," Frontiers in Neuroscience, vol. 12, p. 00186, 2018.

[16] Raspopovic, S., et al, "A computational model for the stimulation of rat sciatic nerve using a transverse intrafascicular multichannel electrode," IEEE Transactions on Neural Systems and Rehabilitation Engineering, vol. 19, no. 4, pp. 333-44, 2011.

[17] Taguchi, K., et al, "Anatomical studies of the autonomic nervous system in the human pelvis by the whole-mount staining method: Left-right communicating nerves between bilateral pelvic plexuses," The Journal of Urology, vol. 161, pp. 320-25, 1999.

[18] Jang, H.S., et al, "Composite nerve fibers in the hypogastric and pelvic splanchnic nerves: an immunohistochemical study using elderly cadavers," Anatomy & Cell Biology, vol. 48, pp. 114-23, 2015.

[19] Grinberg, Y., et al, "Fascicular perineurium thickness, size, and position affect model predictions of neural excitation," IEEE Transactions on Neural Systems and Rehabilitation Engineering, vol. 16, no. 6, pp. 572-81, 2008.

[20] M. Swallow, "Fibre size and content of the anterior tibial nerve of the foot," Journal of Neurology, Neurosurgery & Psychiatry, vol. 29, no. 3, pp. 205-13, 1966.

[21] Chopra, J.S. & Hurwitz, L.J, "Sural nerve myelinated fibre density and size in diabetics," Journal of Neurology, Neurosurgery & Psychiatry, vol. 32, pp. 149-54, 1969.

[22] P. Donker, "A study of the myelinated fibres in the branches of the pelvic plexus," Neurourology and Urodynamics, vol. 5, pp. 185-202, 1986.

[23] Amin, T.N., et al, "Reference ranges for uterine vein dimensions in non-pregnant women with normal pelvic organs," Ultrasound in Obstetrics & Gynecology, vol. 54, pp. 403-11, 2019.

[24] Katahira, A., et al, "Intraoperative electrical stimulation of the pelvic splanchnic nerves during nerve-sparing radical hysterectomy," Gynecologic Oncology, vol. 98, pp. 462-66, 2005.

[25] Possover, M., et al, "Anatomy of the sacral roots and the pelvic splanchnic nerves in women using the LANN technique," Surgical Laparoscopy Endoscopy & Percutaneous Techniques, vol. 17, no. 6, pp. 508-10, 2007.

[26] Sweeney, J.D., et al, "Modeling of mammalian myelinated nerve for functional neuromuscular stimulation," IEEE Transactions on Biomedical Engineering, vol. 40, no. 12, pp. 1201-9, 1993.

[27] Raspopovic, S., et al, "Framework for the development of neuroprostheses: From basic understanding by sciatic and median nerves models to bionic legs and hands," Proceedings of the IEEE, vol. 105, no. 1, pp. 34-49, 2017.

[28] Veltink, P.H., et al, "A modeling study of nerve fascicle stimulation," IEEE Transactions on Neural Systems and Rehabilitation Engineering, vol. 36, pp. 683-92, 1989.

[29] Geddes, L.A. & Baker, L.E., "The specific resistance of biological material- A compendium of data for the biomedical engineer and physiologist," Medical and biological engineering, vol. 5, pp. 271-93, 1967.